

## SENSITIVITY ANALYSIS OF THE THREE DIMENSIONAL FLOW DYNAMICS IN THE CONTINUOUS CASTING SUBMERGED ENTRY NOZZLE

Cesar Real<sup>a</sup>, Luis Hoyos<sup>b</sup>, Francisco Cervantes<sup>b</sup>, Raul Miranda<sup>c</sup>, Manuel Palomar-Pardavé<sup>a</sup>, and Jesus Gonzalez<sup>b</sup>

<sup>a</sup>Departamento de Materiales, Universidad Autónoma Metropolitana - Azcapotzalco, San Pablo 180, Col. Reynosa-Tamaulipas, Del. Azcapotzalco C. P. 02200, México, D.F. México.

<sup>b</sup>Departamento de Sistemas, Universidad Autónoma Metropolitana - Azcapotzalco, San Pablo 180, Col. Reynosa-Tamaulipas, Del. Azcapotzalco C. P. 02200, México, D.F. México. Email:

[gtji@correo.azc.uam.mx](mailto:gtji@correo.azc.uam.mx)

<sup>c</sup>Departamento de Electrónica, Universidad Autónoma Metropolitana - Azcapotzalco, San Pablo 180, Col. Reynosa-Tamaulipas, Del. Azcapotzalco C. P. 02200, México, D.F. México.

**Keywords:** Continuous casting, dynamical behavior, submerged entry nozzle, pool geometry, flow patterns, numerical solution.

**Abstract.** Many quality problems that originate during continuous casting can be directly attributed to poor control of fluid flow conditions, fluctuations on flow rate from the ladle into the mold cavity and changes on nozzle exit port flow patterns. The objective of this study is to characterize the dynamical behavior of the mold Submerged Entry Nozzle (SEN) based on computational models. The numerical results validation was performed by direct comparison with experimental data. A commercial code based on the finite volume method was used to solve this problem. The Large Eddy Simulation (LES) turbulence model was used in this work. It was observed that numerical solution is sensible to variations on solution method parameters and modifications of the nozzle bottom geometry. For instance, when the gradient calculation was based on the cell, the solution converges to a stable stationary point. On the other hand, when the gradient calculation was based on the node, the solution converges to a limit cycle. Additionally, it was observed that slight variations in the nozzle pool geometry leads to different mold entrance flow patterns.

## 1 INTRODUCTION

The Continuous Casting Process (CCP) is used to solidify most of the one thousand two hundred and forty-four million metric tons of steel and many other metals and alloys produced in the world yearly ([World of Steel in Figures, 2006](#)). One of the most important aspects of this process is the delivery of steel into mold. A typical two port Submerged Entry Nozzle (SEN) used in thick slab casters has a horizontal angle. This angle contributes to modify the flow pattern inside the mold. The most common configuration is a  $15^\circ$  downward angle, nevertheless, even upward angles may be employed. The main components of a CCP mold are shown in [Figure 1](#).

In the CCP, the molten metal flows from a ladle, into the mold through a tundish. The steel should be protected from exposure to air by a slag cover over each vessel and by ceramic nozzles between the vessels. Once in the mold, the molten steel freezes against the water-cooled copper mold walls to form a solid shell. Below the mold exit, the solidifying steel acts as a container to support the remaining liquid. Drive rolls continuously withdraw the shell from the mold at a rate of “casting speed” which matches the flow of incoming metal. Ideally, the process runs in steady state, but there are several operating conditions that can change the initial supposition. The rolls support the steel to minimize bulging due to the ferrostatic pressure. To reduce the strand surface temperature, water and air mist sprays between rolls are used until the molten core has been solidified. Once the center is completely solidified, the strand can be cut into slabs.

Several important phenomena which govern the CCP and determine the quality of the product, originates in the nozzle. Depending on the SEN exit flow pattern, the steel jet emerging from the SEN may collide against the mold walls in different ways. In the mold, the steel jet generates two recirculation regions in the molten metal: an upper and a lower recirculation regions ([Kamal and Sahai, 2006](#)). The upper part contributes to the formation of surface waves and turbulence. While the lower part determines the hydrodynamics in the mold, the solidified shell, and heat transfer process ([Real et al., 2007b](#)).

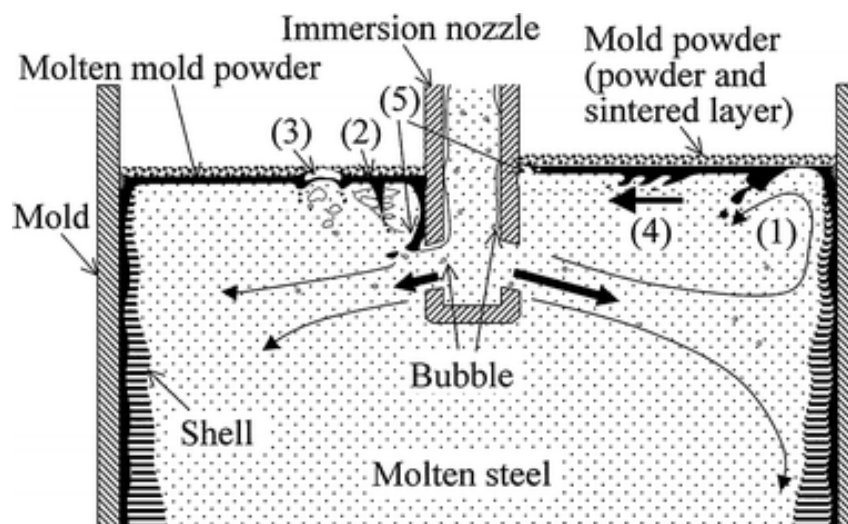


Figure 1: Main features of a continuous casting mold ([Zhang et al., 2007](#)). Types of mold powder entrapment (1)

Flow reversing from the narrow face of the mold, (2) Kelvin- Helmholtz instability, (3) Karman vortex streets shed regularly behind the SEN, (4) Attack of argon bubbles coming from the SEN ports, (5) Uneven discharging flow, the mold powder descends along the outer surface of the SEN due to pressure decrease on the rear surface of the SEN.

Many important aspects of the hydrodynamics in CCP mold are transient and difficult to control, due to its turbulent nature. However, the flow pattern in the mold is greatly influenced by SEN geometry, SEN submergence depth, mold dimensions, argon injection rate, and electromagnetic forces. The changes in SEN geometry are inexpensive; but these changes have a critical influence on steel quality.

The fluid flow inside the SEN, has been studied by several authors using for instance numerical simulations (Real et al., 2007a; Real et al., 2007b; Zhang et al., 2007; Zhang et al., 2006; Kamal et al., 2006; Ramirez et al., 2005; Li et al., 2005) and water based physical models (Zhang et al., 2007; Kamal et al., 2006; Li et al., 2005; Miranda et al., 2005).

To reduce the computational effort, most of the numerical simulations have used the  $\kappa$ - $\epsilon$  or the Reynolds Stress Model (RSM) turbulence models. In several of these works, there is neither coincidence with plant observations nor with physical simulations. To improve their results, secondary process elements such as the tundish sliding gate and the SEN argon injection have been used in different works. On the contrary, it has been shown that using the correct turbulence model (Real et al., 2007a; Real et al., 2007b; Real et al., 2006), the physical and the plant results can be reproduced without the secondary elements previously mentioned.

Additionally, the effect of some SEN geometrical elements on the mold flow pattern is not fully understood. The most controversial element is the SEN pool. Some authors have pointed out that a recessed SEN (with pool), increases the mold surface turbulence and therefore the presence of non-metallic inclusions in the product (Zhang et al., 2007a; Thomas et al., 2002; Thomas et al., 2001a; Yokoya et al., 2001; Bai and Thomas, 2001a; Bai and Thomas, 2001b). Other authors have also mentioned that a flat bottom SEN (without pool), produces the above mentioned effect (Thomas et al., 2001b; Kubo et al., 2001; Brummayer et al., 1999). On the other hand, the effect of the pool is considered as negligible by other authors (Yokoya et al., 1998).

This paper has two main objectives. The first one is to show that the turbulence model as well as the numerical method must be correctly selected to reproduce the reported behavior in the SEN. To accomplish this, the numerical simulations of a recessed SEN using LES and two different gradient calculations are compared. The second objective is to determine the influence of the bottom geometry on the SEN flow pattern. This is done by numerical simulations of three different SEN bottom geometries and comparing these results with water based physical simulations.

## 2 MATHEMATICAL MODEL

### 2.1 General Equations

The governing equations employed for LES are obtained by filtering the time-dependent Navier-Stokes equations (Fluent, 2007) obtaining:

$$\frac{\partial \rho}{\partial t} + \frac{\partial}{\partial x_i} (\rho \bar{u}_i) = 0 \quad (1)$$

$$\frac{\partial}{\partial t} (\rho \bar{u}_i) + \frac{\partial}{\partial x_j} (\rho \bar{u}_i \bar{u}_j) = -\frac{\partial}{\partial x_j} (\mu \sigma_{ij}) - \frac{\partial \bar{p}}{\partial x_i} - \frac{\partial \tau_{ij}}{\partial x_j} \quad (2)$$

Where  $\sigma_{ij}$  is the stress tensor due to molecular viscosity,  $\tau_{ij}$  is the subgrid-scale stress

defined by  $\tau_{ij} \equiv \overline{\rho u_i u_j} - \rho \bar{u}_i \bar{u}_j$ .

The variables involved are defined in the nomenclature section. The overbar denotes a filtered variable.

## 2.2 LES Turbulence Model

In recent years, Large Eddy Simulation (LES) turbulence model has been employed in engineering applications to analyze complex transient fluid flows. On the contrary to the  $\kappa$ - $\epsilon$  turbulence model which yields time-averaged results, LES yields fine details of the time-dependent flow structures (Eriksson et al., 2004; Thomas et al., 2001a). To carry out properly its task, LES requires extremely fine grids and very small time steps which significantly increases the computational effort.

In LES, only the turbulent flow eddies which can be resolved by the computational grid are computed and those which are unresolved are only modeled (Eriksson et al., 2004). In this work, to model the unresolved flow structures, the Smagorinsky-Lilly model was employed (Fluent, 2007). The subgrid-scale turbulent stresses are given by:

$$\tau_{ij} = \frac{1}{3} \tau_{kk} \delta_{ij} - 2 \mu_t \bar{S}_{ij} . \quad (3)$$

The rate-of-strain tensor for the resolved scale is defined by:

$$\bar{S}_{ij} = \frac{1}{2} \left( \frac{\partial \bar{u}_i}{\partial x_j} + \frac{\partial \bar{u}_j}{\partial x_i} \right) . \quad (4)$$

In the Smagorinsky-Lilly model, the eddy-viscosity is modeled by:

$$\mu_t = \rho L_s^2 |\bar{S}| , \quad (5)$$

where the mixing length for subgrid scales  $L_s$  and  $|\bar{S}|$  is calculated as:

$$L_s = \min(\kappa d, C_s V^{1/3}) , \quad (6)$$

and

$$|\bar{S}| \equiv \sqrt{2 \bar{S}_{ij} \bar{S}_{ij}} . \quad (7)$$

$C_s$  is not an universal constant, which is the most serious shortcoming of this model. Nonetheless,  $C_s$  value of around 0.1 has been found to yield the best results for a wide range of flows.

## 2.3 Boundary conditions

The hydrodynamic study was performed using the Large Eddy Simulation (LES) turbulence model to simulate water as working fluid. The inlet velocity condition where set without perturbation and constant magnitude of 1.45 m/s. The outlet condition was defined as outflow on both SEN exit ports. Other boundary conditions involve non-slip flow at walls. The total number of elements employed in the model ensured a stable computing. The under-relaxing coefficients for momentum and pressure were 0.7 and 0.3 respectively. The pressure-velocity coupling was SIMPLE. Convergence was reached when all residuals of the turbulence flow was smaller than  $1 \times 10^{-3}$ . Convergence study was done by using  $1.0 \times 10^6$ ,  $1.25 \times 10^6$  and  $1.5 \times 10^6$  elements and no significant changes were observed.

### 3 RESULTS AND DISCUSSION

#### 3.1 Model description

The mathematical model equations were solved using commercial CFD software. The simulation with LES turbulence model requires a large quantity of elements. Therefore, the three models used, have approximately 1,500,000 elements. In all simulations, the time step employed was 0.001 s. To accomplish 12 s of real time process, the numerical simulation required approximately 100 hrs of CPU time on one workstation with two Opteron 2.0 Ghz dual core processors with 6 GB of RAM memory and 400GB hard disk using Linux platform.

DIMENSIONS	VALUE
SEN bore diameter	0.0254 m
Port diameter	0.02 m
Port thickness	0.012 m
Port angle (downward from horizontal)	15°
Model height	0.30 m
Pool depths	0, 0.02 m
SEN inlet velocity	1.45 m/s

Table 1: Model geometric dimensions.

The mathematical model presented in the previous section can be solved using liquid steel as the working fluid. However, validation of the numerical results is not feasible due to the few CCP data available. To overcome this limitation, extensive work has been done by employing physical water models to investigate the fluid flow phenomena in the mold region of the CCP (Teshima et al., 1993; Gupta et al., 1997). In those works, a similarity criterion was used to design the water model. The Reynolds, Weber, and Froude criterion are commonly used. The similarity criterion ensures that the results obtained in the scaled model can be extrapolated to the current CCP mold.

The numerical simulations carried out in this work employed water as the working fluid. Additionally, the Froude similarity criterion was used to construct a 1/3-scale model. To reproduce a typical casting rate, the water inlet flow rate was 44 l/min. The SEN dimensions used in this work are shown earlier in Table 1. The unique difference between them was the pool depth. All numerical simulations were performed under transient conditions.

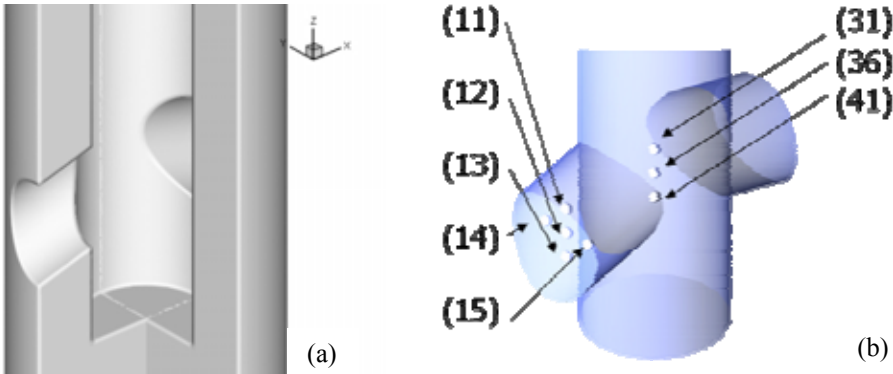


Figure 2: (a) Schematic representation of a recessed SEN. (b) Spatial location of the monitoring points.

The magnitude velocity was recorded in fifty measurement points, however, only the results of eight selected points are presented. The spatial distribution of these points is shown in [Figure 2](#) and their coordinates are reported in [Table 2](#). At one of the SEN exit ports, points 11 to 15 were located in the middle. While the points 31, 36 and 41 were located in the center of the SEN. The information provided at these points is enough to understand the fluctuations observed inside the SEN, and therefore, at the exit port. Additionally, previous works showed that the most important flow modifications takes place in a section close to the exit ports and the pool ([Real et al., 2006](#)).

Point	X (cm)	Y (cm)	Z (cm)
11	2.070	1.286	0.000
12	2.070	0.786	0.000
13	2.070	0.286	0.000
14	2.070	0.786	-0.500
15	2.070	0.786	0.500
31	0.000	0.500	0.000
36	0.000	1.000	0.000
41	0.000	1.500	0.000

Table 2: Spatial position of the monitoring points.

### 3.2 Evaluation of the gradient calculation effect

The numerical simulations, when the gradient calculation was based on the node are shown in [Figures 3](#) and [4](#). The results when the gradient calculation was based on the cell are presented in [Figures 5](#) and [6](#).

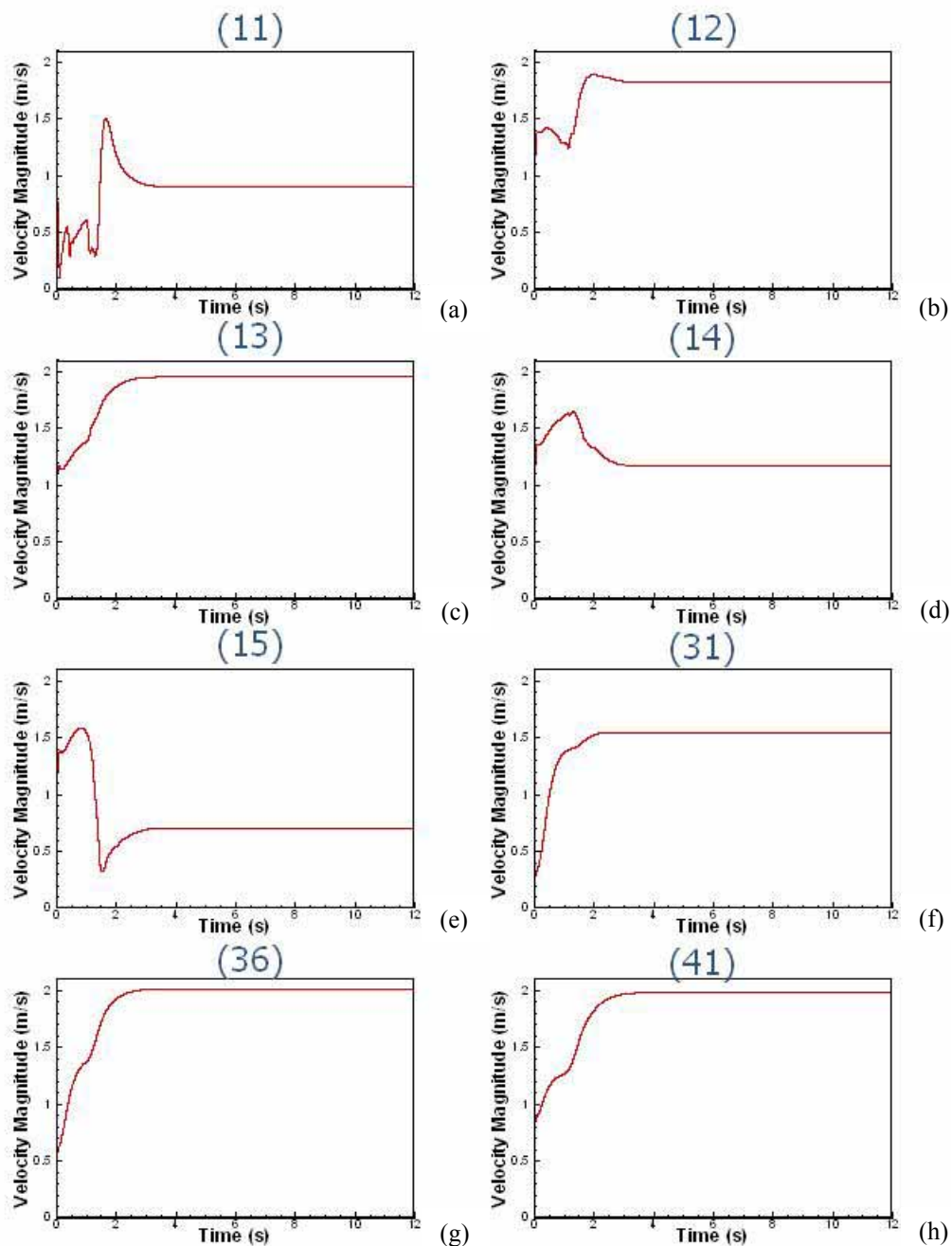


Figure 3: Velocities time series at the monitoring points with gradient calculation based on the node.

Figures 3 and 5 show the velocity time series at the measurement points reported in Table 2. It can be observed that in both cases there is a transitory behavior in the early stages. Afterward, the flow conditions inside the SEN evolve to a quasi-steady state structure when the gradient calculation is based on the node (see Figure 3). On the contrary, a limit cycle of the flow pattern inside the SEN appears when the gradient calculation is based on the cell.

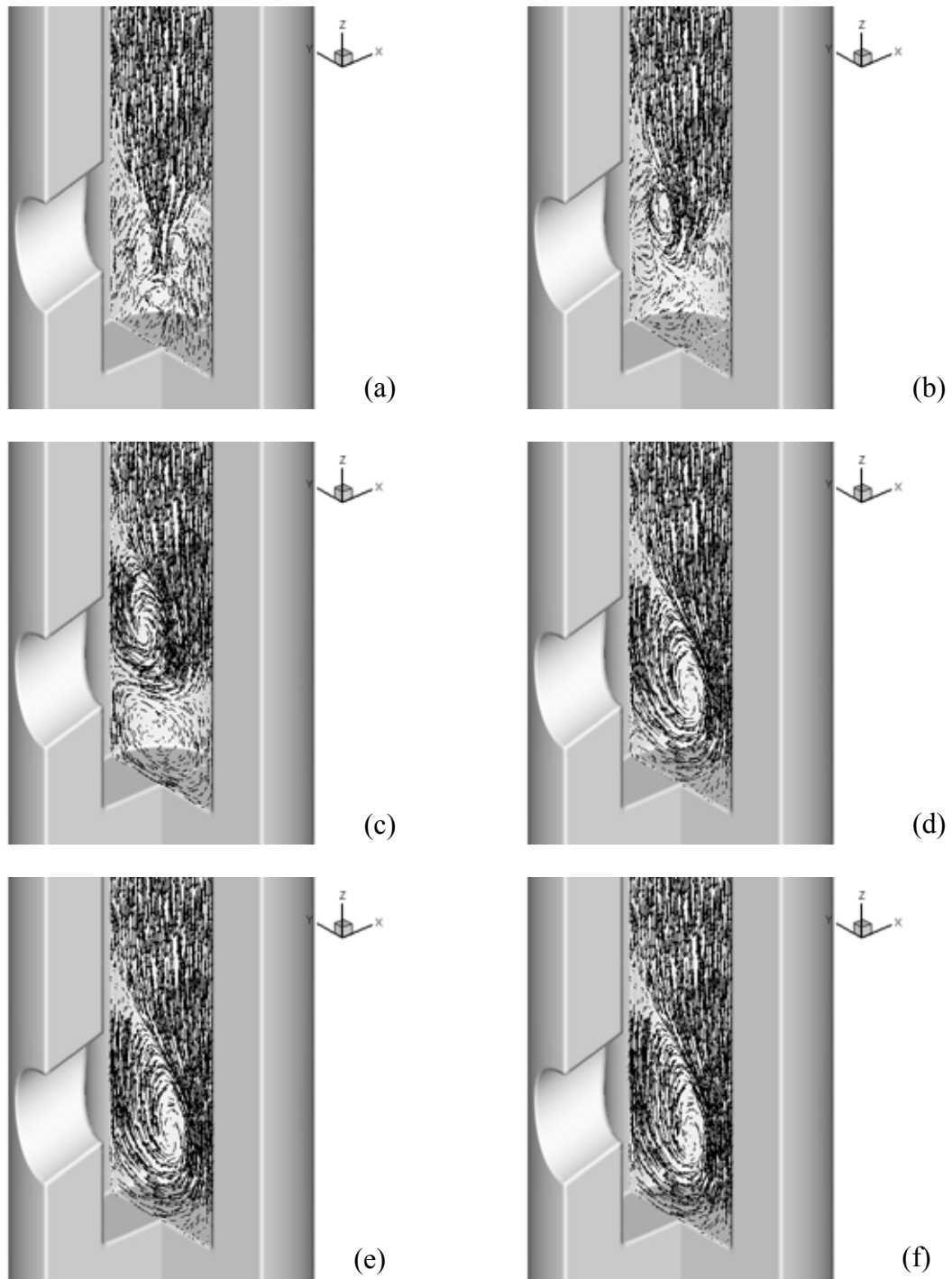


Figure 4: Flow behavior inside the recessed SEN with gradient calculation based on the node at several simulation times. (a) 0.5 s. (b) 1.0 s. (c) 1.5 s. (d) 3.5 s. (e) 5.0 s. (f) 12.0 s.

The analysis of the exit port zone when the gradient calculation is based on the node is as follows. The center point (12) has the highest velocity magnitude. With respect the vertical plane, the exit flow pattern is asymmetric. The velocity magnitude at point (14) is double the velocity magnitude at point (15). This is due to the flow pattern, having a predominant clockwise vortex which occupies the entire pool volume and therefore determines the flow pattern in the port. This behavior can also be used to explain the raise in the velocity magnitude from points (31) to (36) and the subsequent drop from points (36) to (41). There is

a considerable difference between the velocity magnitudes in the lower point (13) and the upper point (11). The velocity magnitude at point (13) is double the velocity magnitude at point (11).

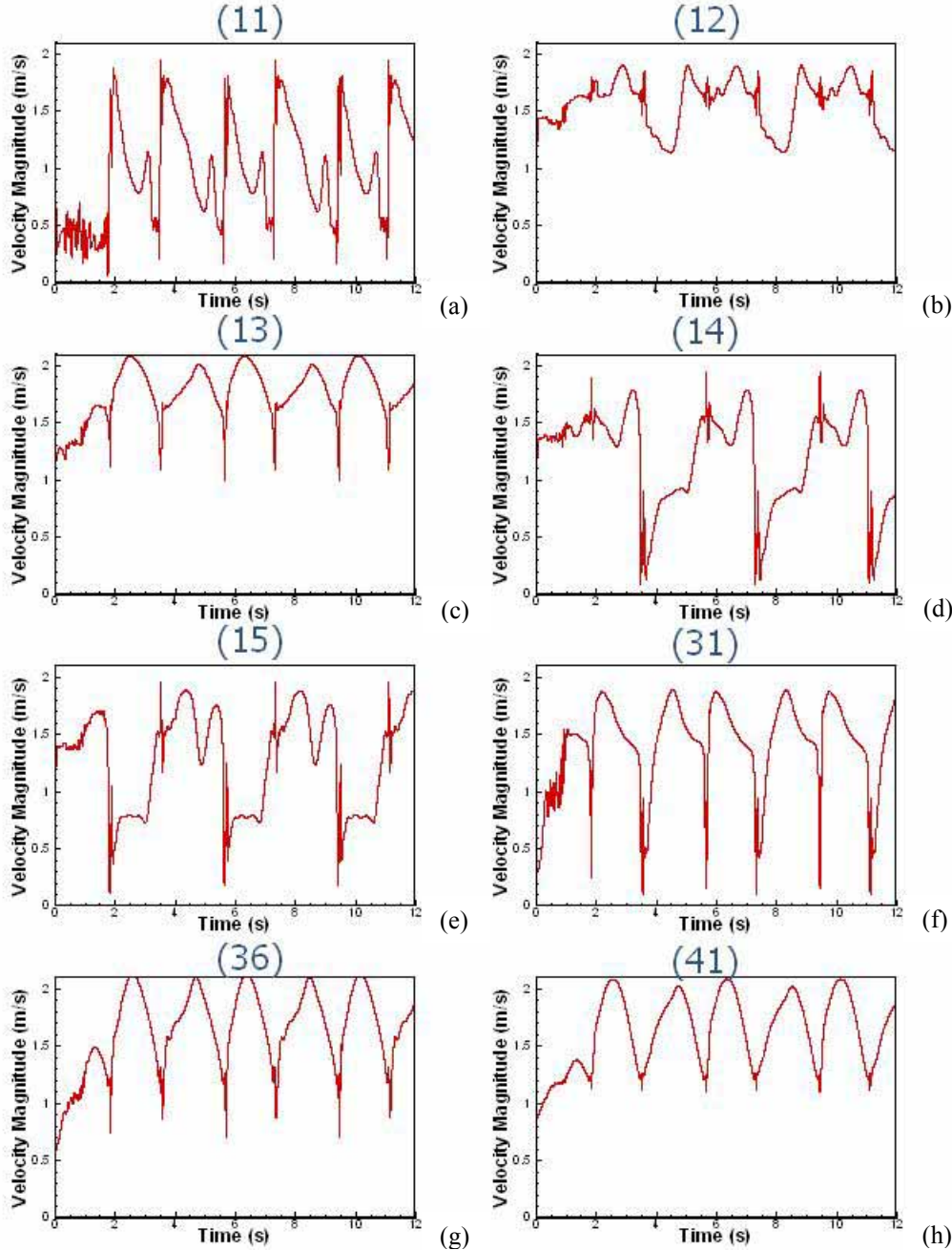


Figure 5: Velocities time series at the monitoring points with gradient calculation based on the cell.

The flow patterns inside the SEN are shown in Figure 4. These flow patterns were reported at different simulation times. Figures 4a-4c show the transitory behavior at early stages. However, it can be observed in Figures 4d-4f, that there are no significant changes in the fluid flow pattern inside the SEN.

Figure 4b and Figure 4c show the formation of two vortices inside the SEN. One of the vortices is located at exit port height, while the other occupies the pool volume. As the process evolves, the lower vortex disappears and the size of the upper vortex increases. During the transient period the SEN exit flow pattern displays variations, but thereafter remains almost unchanged.

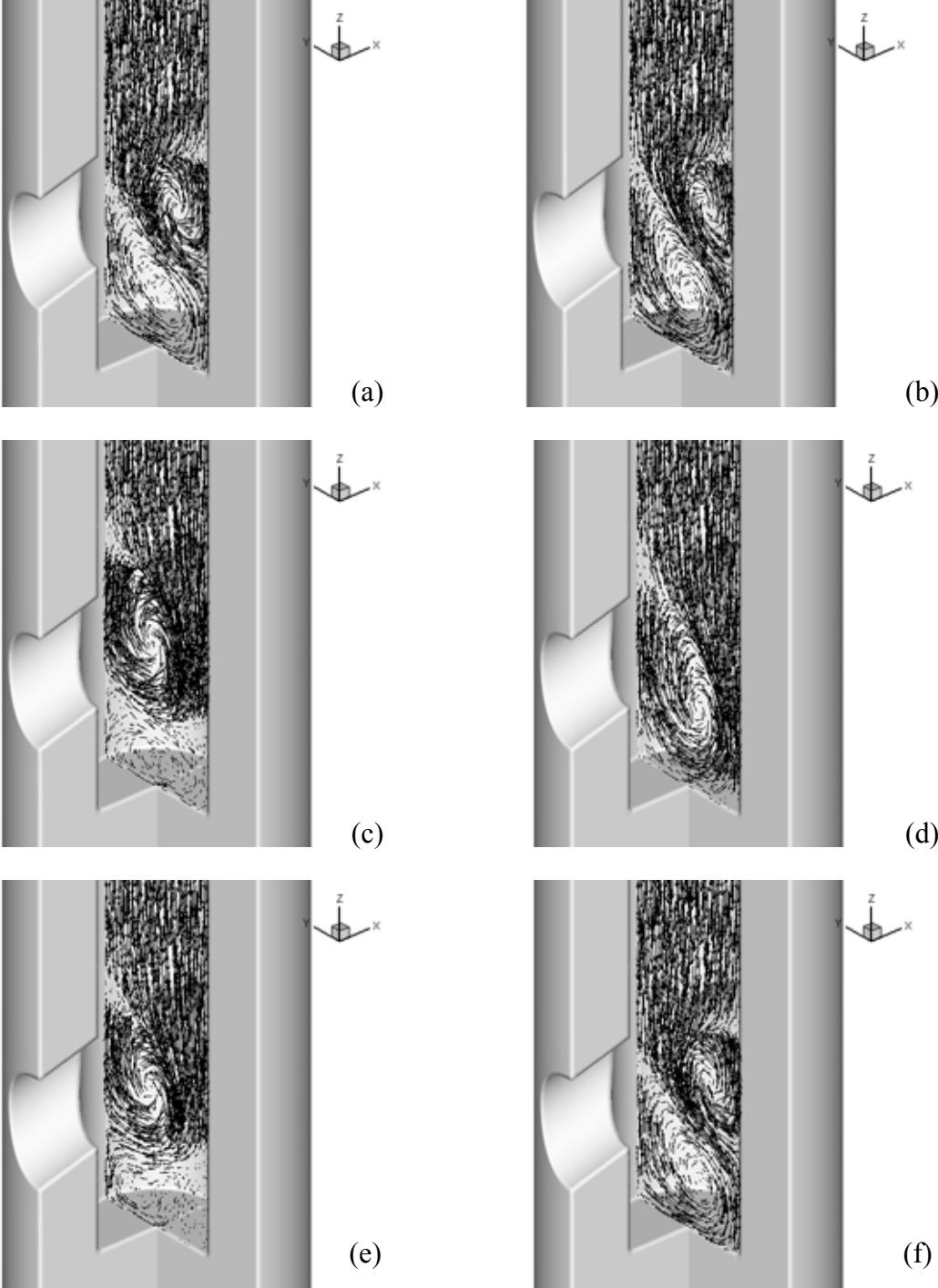


Figure 6: Flow behavior inside the recessed SEN with gradient calculation based on the node at several simulation times. (a) 0.5 s. (b) 1.0 s. (c) 1.5 s. (d) 3.5 s. (e) 7.0 s. (f) 10.0 s.

The Figure 5 and 6 show the numerical simulations when the gradient calculation was

based on the cell. Once the early transitory behavior has finished, a well established periodical behavior emerges, this is shown in Figure 5. It must be highlighted that the amplitude of the velocity magnitude variations is considerable high. The highest variations are observed at points (11), (14), (15) and (31). These points are located in the upper exit-port middle part. It can also be observed that the fluctuations frequency is the same at all the monitoring points. Nevertheless, the local minimum and the local maximum do not occur at the same time at all the monitoring points.

The mean average of data showed in Figure 5 almost corresponds to the data shown in Figure 3. In other words, when the gradient calculation is performed on the node, high frequency fluctuations are filtered, therefore a quasi-steady state is obtained.

With the results presented in this subsection, it can be concluded that gradient calculation based on the cell is a better option in the simulation of the behavior inside the SEN of a CCP mold when the turbulence model used is LES.

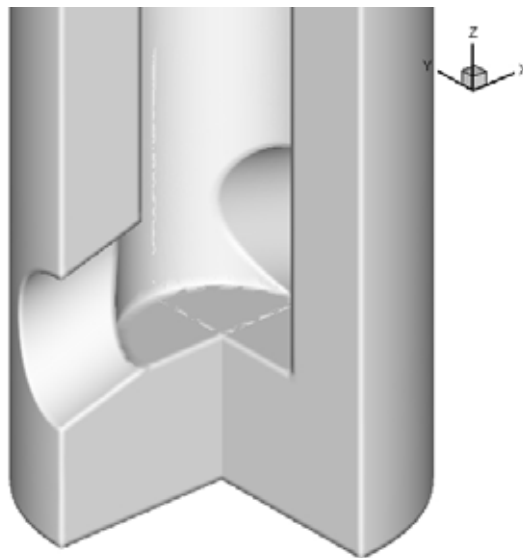


Figure 7: Schematic representation of a flat bottom SEN.

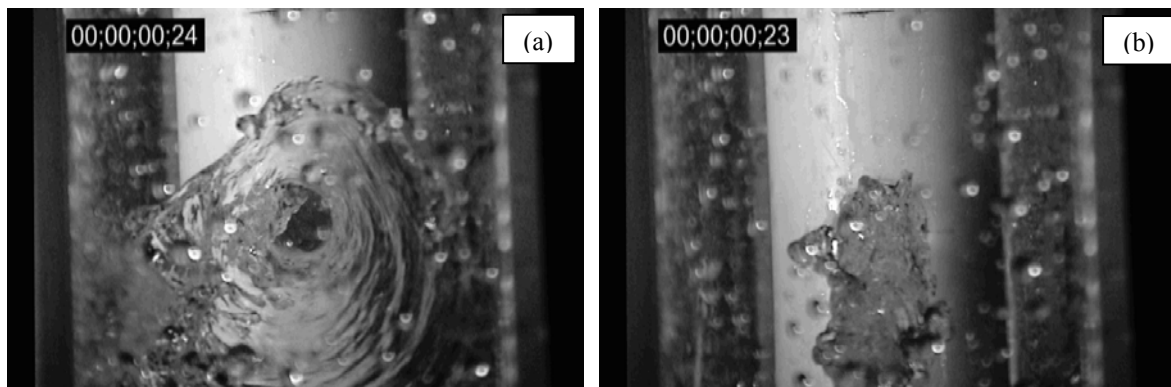


Figure 8: Flow pattern of the exit jet SEN. (a) Recessed SEN. (b) Flat bottom SEN.

### 3.3 Evaluation of the pool effect

The analysis of the SEN pool effect on the flow pattern at SEN exit ports becomes significant due to clogging. Nozzle clogging is a natural phenomenon in casting steels which contain inclusions. It can also be seen in steel containing solid or semi-solid inclusions which

can precipitate. There are two types of clogs, thermal and inclusional. The second is a consequence of the agglomeration of a present inclusion or precipitation of inclusions. Both types are very sensitive to fluid flow conditions. However, agglomeration clogs can be minimized by ladle metallurgy practices, while precipitation clogs are very sensitive to local thermal conditions and compatibility with the SEN (Thomas and Yu, 2002).

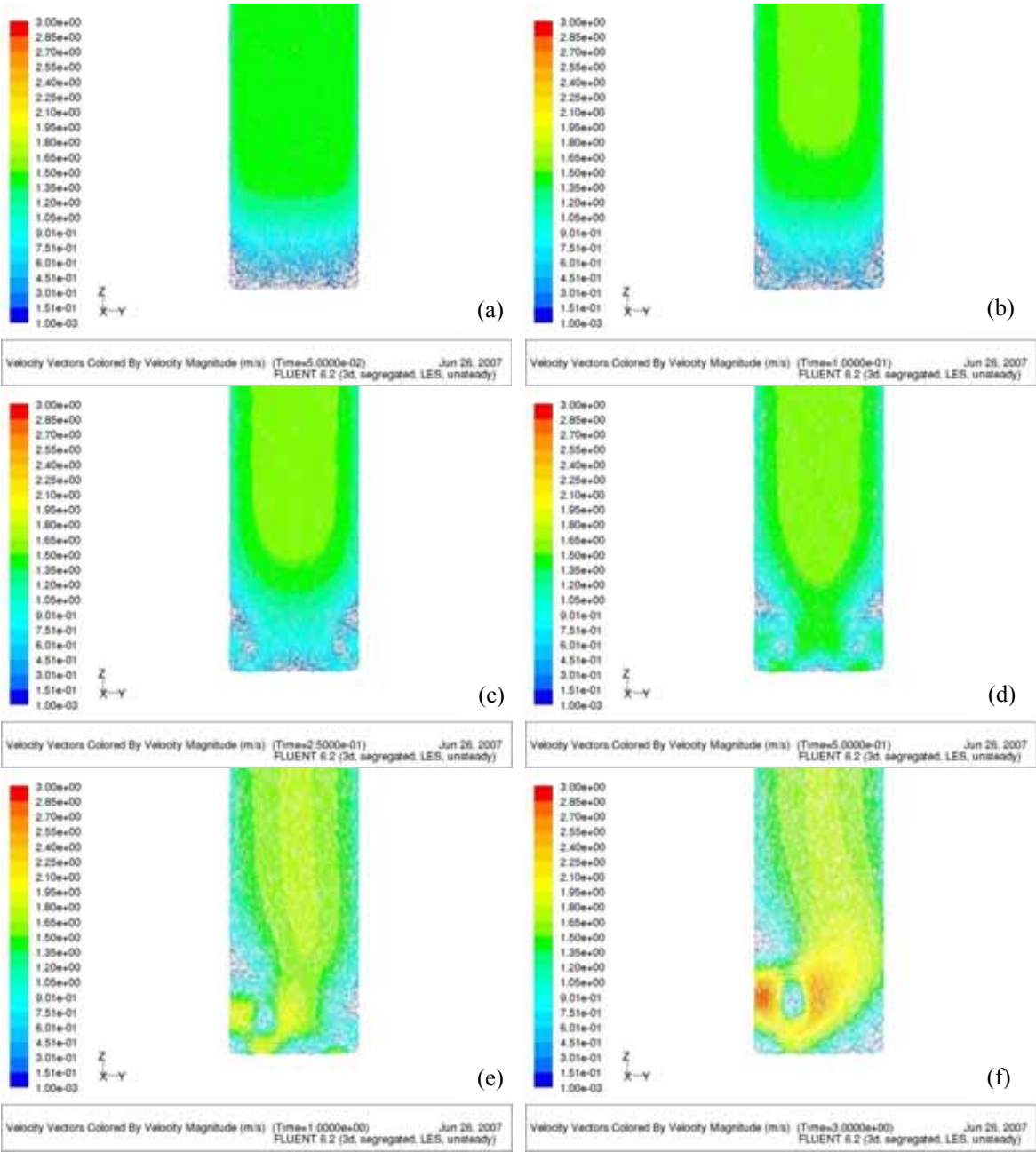


Figure 9: Dynamics of the flow pattern inside the flat bottom SEN. The simulation time is indicated of each figure.

Clogging alters the SEN internal geometry. Generally, agglomeration clogs tends to settle where the steel velocity is slow, for instance, at the SEN pool. When clogging is excessive, a recessed SEN becomes a flat bottom one, as that shown in Figure 7. This transition is gradual and it is very difficult to determine the SEN clogging extent.

In several works, recessed and flat bottom SEN have been studied (Thomas et al., 2001a;

Kubo et al., 2001; Brummayer et al., 1999). However, it is not permitted with the available data to elucidate the real effect of the bottom geometry on the flow pattern inside the SEN. Therefore, on the behavior inside the CCP mold. To emphasize this effect, non traditional physical experiments were carried out using a recessed (see Figure 2) and a flat bottom SEN (see Figure 7). In these experiments, SEN discharges in a half-filled mold. A representative sample of each experiment is shown in Figure 8. The shape of the water jet for each SEN is notably different. A flat bottom SEN produces a very narrow jet. On the contrary, the recessed SEN produces a very wide jet. Another important difference between them is that the narrow jet directly collides against narrow wall of the mold whereas the wide jet collides mainly on the wide walls.

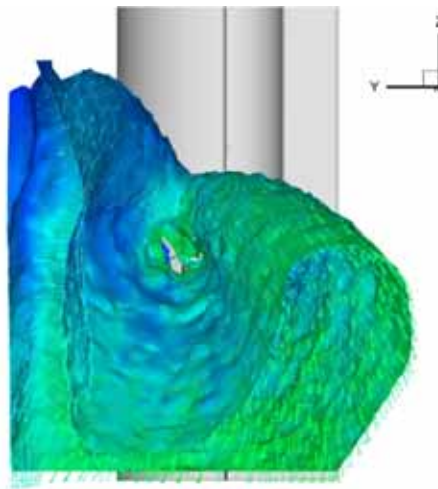


Figure 10: Schematic representation of a flat bottom SEN.

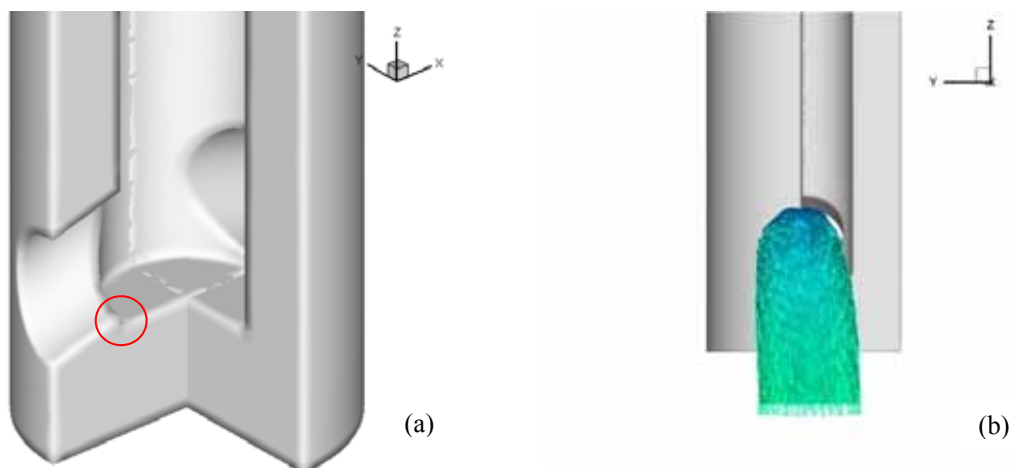


Figure 11: Transient flow pattern on "mini pool" SEN.

It is well known that the way the steel jet collides against the mold walls modifies the solid steel shell formed in the mold. If the shell is extremely thin, slabs with severe surface defects are obtained. The characterization of this phenomenon is out of the scope of this work, but this finding deserves further investigation.

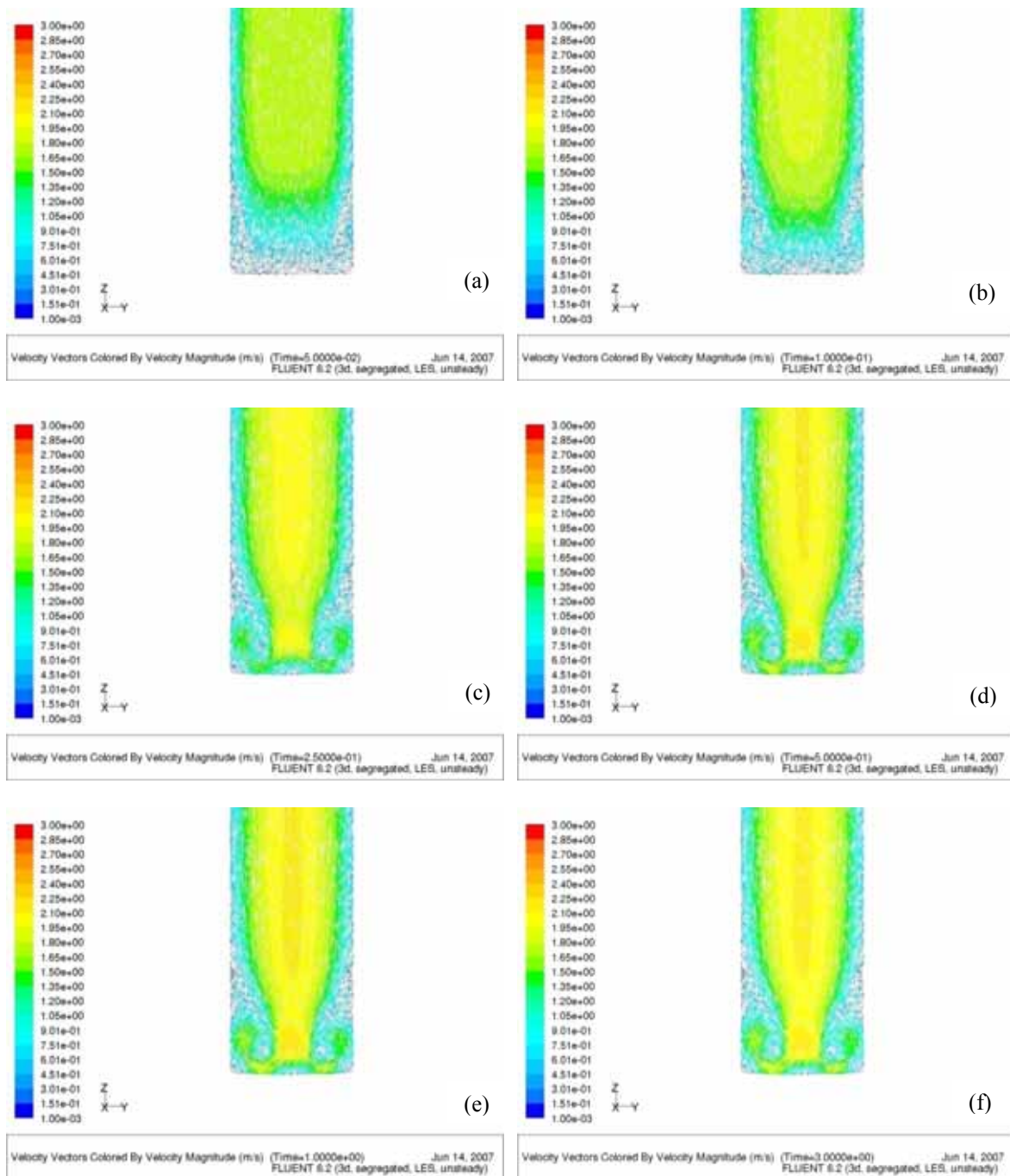


Figure 12: Velocity vectors by magnitude “mini pool” SEN.

Figure 9 shows the dynamic behavior of the central flow pattern inside the flat bottom SEN. Each figure indicates the corresponding simulation time. Figures 9a-9d shows the initial transient behavior. Figure 9e and Figure 9f shows a quasi-steady state is reached. The flow pattern shown in Figure 9f is similar to that shown in Figure 4f.

The SEN discharge to the empty mold was numerically simulated using the SEN exit port flow pattern obtained from the previous simulation. The results of this simulation can be seen in Figure 10. It can be observed that the shape of the simulated jet, matches with that obtained with a recessed SEN (Figure 8a).

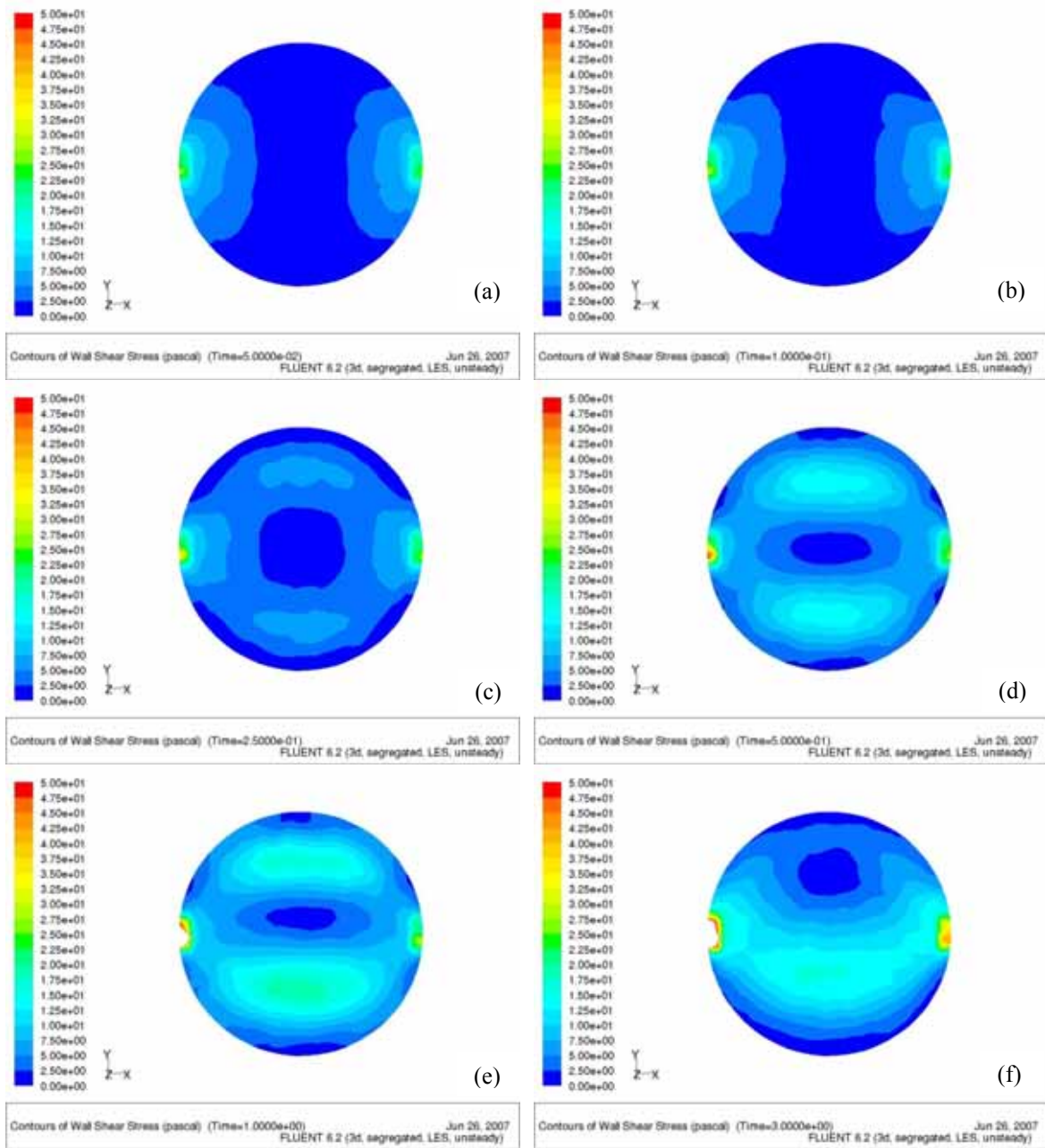


Figure 13: Contours of wall shear stress on the bottom for the recessed SEN.

To reproduce the behavior observed in physical simulations using a flat bottom SEN, a modification on the internal geometry was explored. Figure 11a shows a SEN with a mini-pool. Notice that the volume of this mini-pool is negligible compared with the SEN interior volume. The mini-pool is used to soften the water impact on the SEN bottom.

Figure 11b shows the SEN discharge to the empty mold using the SEN exit port flow pattern obtained with the mini-pool. In this case the agreement between numerical and physical simulations is outstanding.

The dynamic behavior of the fluid flow pattern inside the SEN for the mini-pool SEN is shown in Figure 12. By comparing Figure 9 and Figure 12, it is clear that the initial transitory is similar for the recessed and the mini-pool SEN. However, in the flat bottom SEN, one of the two vortexes at the bottom begins disappearing after 1 second. Afterwards, the flow inside the SEN is significantly different for both nozzles.

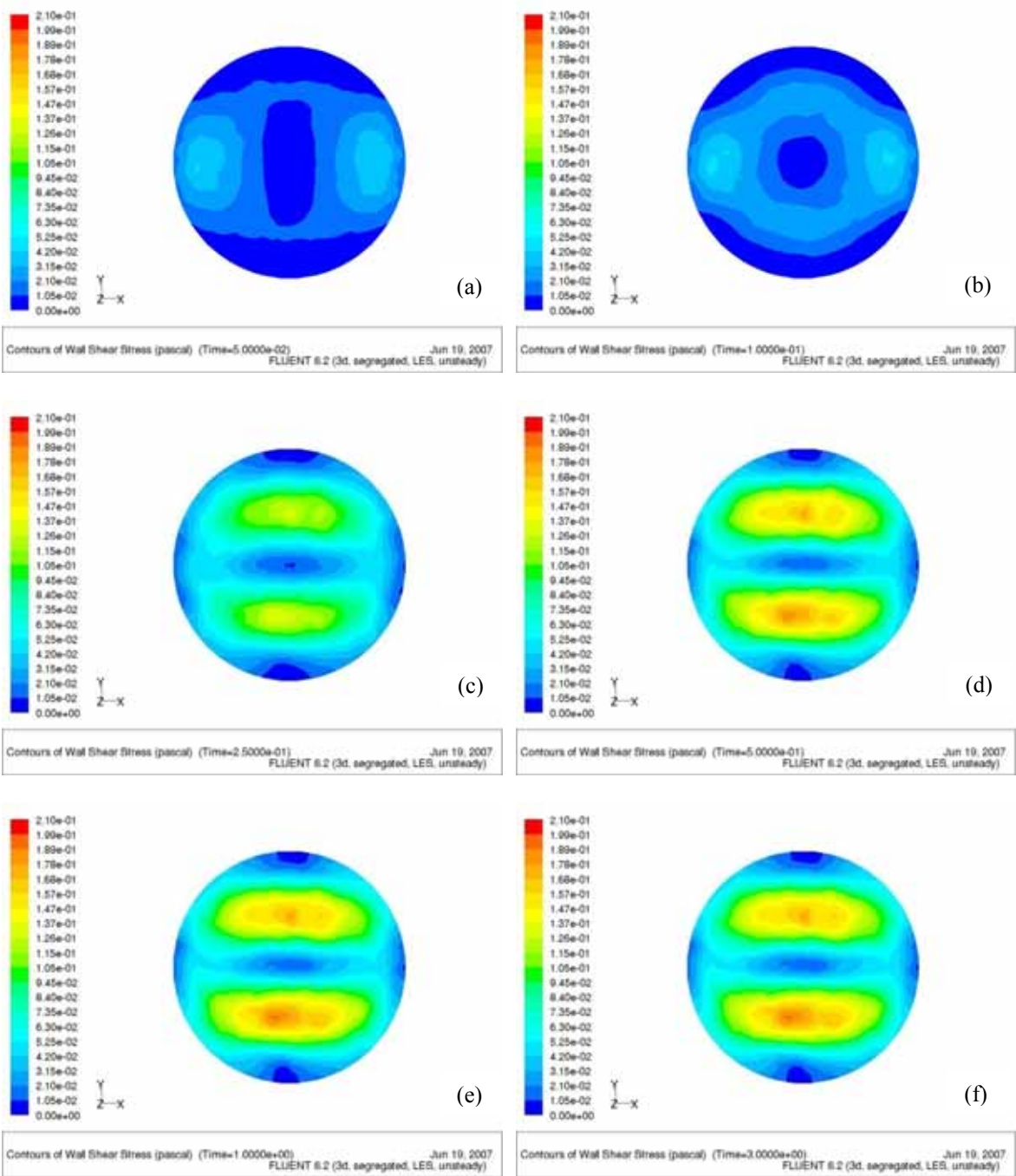


Figure 14: Contours of wall shear stress on the bottom for the mini-pool SEN.

The effectiveness of the mini-pool can be evaluated, by calculating the wall shear stress at the SEN bottom. The results for the recessed and the mini-pool SEN are shown in [Figure 13](#) and [Figure 14](#) respectively. These figures show the dynamic behavior of the wall shear stress contours at the SEN bottom.

Evidently the shape of the wall shear stress contours is different for each SEN. In the flat bottom SEN, the biggest stresses are located at the exit ports beginning. On the contrary, located at the same position are the smallest stresses in the mini-pool SEN.

The most important difference between the wall shear stress contours obtained with the flat bottom and the mini-pool SEN is the magnitude. The wall shear stress ranges from 0 to 50 Pa in the flat bottom SEN, and ranges from 0 to 0.21 Pa in the mini-pool SEN. This means that the largest wall shear stress in the flat bottom pool is approximately two hundred times the largest one in the mini-pool SEN. This difference confirms that the mini-pool weakens the fluid impact in the SEN bottom.

#### 4 CONCLUSIONS

This work analyzed two fundamental aspects for numerical simulation of the CCP mold SEN. It was showed that unrealistic results were obtained when some numerical method parameters were not well selected, despite the complexity of the turbulence model. It was also observed that minor modifications on the internal SEN geometry could produce significant differences on the numerical simulation results.

To reproduce the behavior of the flat bottom SEN, an artificial mini-pool was employed. The mini-pool was used to soften the water impact on the SEN bottom. With the mini-pool, the similarity between numerical and physical simulations was good. The underlying principle of the mini-pool becomes significant in current CCP, where gas argon is injected into the SEN. When there are many argon bubbles present at the SEN bottom, its real effects resembles that of the mini-pool.

#### ACKNOWLEDGMENTS

Cesar Real (C.R.) thanks to Consejo Nacional de Ciencia y Tecnología (CONACyT) for grant No. 173354 and FIDERH (Banco de México) for grant No. 05011110152. The numerical simulations were performed in the Laboratorio de Computo Científico del Departamento de Sistemas at Universidad Autónoma Metropolitana (UAM), Azcapotzalco. This work was done with funds from UAM projects numbers 2270303 and 2260220. Special thanks are given to Jacqueline Catherine Alexander for her technical support.

#### NOMENCLATURE

Symbol	Property
$\rho$	Density, $kg \cdot m^{-3}$
$u$	Velocity, $m \cdot s^{-1}$
$t$	Time, $s$
$x, y, z$	Spatial coordinate, $m$
$\Delta$	Change in variable, final-initial, $\Delta x, \Delta y, \Delta z$
$p$	Pressure, $Pa$
$\mu$	Dynamic viscosity, $Pa \cdot s$
$\mu_t$	Eddy viscosity, $Pa \cdot s$
$S$	Strain tensor, $s^{-1}$
$L$	Mixing length, $m$

$\sigma_{ij}$	Stress tensor due to molecular viscosity, $s^{-1}$
$\tau_{ij}$	Subgrid-scale stress, $Pa$
$\delta_{ij}$	Kronecker delta function
$\kappa$	von Kármán constant
$d$	Distance to the closest wall, $m$
$V$	Volume of computational cell, $m^3$

## REFERENCES

- Bai H. and Thomas B.G., Turbulent flow of liquid steel and argon bubbles in slide-gate tundish nozzles: Part I. Mold development and validation, *Metallurgical and Materials Transactions B*, Vol. 32b, 253-267, 2001a.
- Bai H. and Thomas B.G., Turbulent flow of liquid steel and argon bubbles in slide-gate tundish nozzles: Part II. Effect of operation conditions and nozzle design, *Metallurgical and Materials Transactions B*, Vol. 32b, 269-283, 2001b.
- Brummayer M., Gittler P., Watzinger J., Stabilization of unsteady turbulent flow in the mold region of a wide slab caster by submerged entry nozzle design optimization with CFD, *Second International Conference on CFD in the Minerals and Process Industries CSIRO*, Melbourne, Australia, 217-222, 1999.
- Eriksson R., Jonsson L., and Jonsson P.G., Effect of Entrance Nozzle Design on the Fluid Flow in an Ingot Mold during Filling, *The Iron and Steel Institute of Japan International*, Vol. 44, 1358, 2004.
- Fluent User's Guide 6.4 Version. *Fluent Incorporated*, Lebanon, NH, 2007.
- Gupta D., Chakaraborty S., and Lahiri A., Asymmetry and Oscillation of the Fluid Flow Pattern in a Continuous Casting Mould: a Water Model Study, *The Iron and Steel Institute of Japan International* Vol. 37, No. 7, 654-658, 1997.
- Kamal M., Sahai Y., A simple innovation in continuous casting mold technology for fluid flow and surface standing waves control, *The Iron and Steel Institute of Japan International*, Vol. 46, 1823-1832, 2006.
- Kubo N., Kubota J., Ishii T., Simulation of sliding nozzle gate movements for steel continuous casting, *The Iron and Steel Institute of Japan International*, Vol. 41 No. 10, 1221-1228, 2001.
- Li B. and Tsukihashi F., Vortexing flow patterns in a water model of slab continuous casting mold, *The Iron and Steel Institute of Japan International*, Vol. 45, No. 1, 30-36, 2005.
- Miranda R., Barron M.A., Barreto J., Hoyos L., Gonzalez J., Experimental and numerical analysis of the free surface in a water model of a slab continuous casting mold, *The Iron and Steel Institute of Japan International*, Vol. 45, No. 11, 1626-1635, 2005.
- Ramirez-Lopez P., Morales R.D., Sanchez-Perez R., Demedices L.G., Davila O., Structure of turbulent flow in a slab mold, *Metallurgical and Materials Transactions B*, Vol. 36b, 787-799, 2005.
- Ramos-Banderas A., Morales R.D., Sánchez-Pérez R., García-Demedices L., Solorio-Díaz G., Dynamics of two phases downwards flows in submerged entry nozzles and its influence on the two-phase flow in the mold, *International Journal of Multiphase Flow* Vol. 31, 643-665, 2005.
- Real C., Hoyos L., Cervantes F., Miranda R., Palomar-Pardave M., Gonzalez J., Dinámica de fluidos en una buza bifurcada y su influencia en un molde de colada continua, 8°. *Congreso Iberoamericano de Ingeniería Mecánica*, Perú, 533-541, 2007a.
- Real C., Hoyos L., Cervantes F., Miranda R., Palomar-Pardave M., Gonzalez J., Influencia de la geometría de la buza sobre la transferencia de calor en un molde de colada continua, 8°.

- Congreso Iberoamericano de Ingeniería Mecánica*, Perú, 837-846, 2007b.
- Real C., Miranda R., Vilchis C., Barrón M., Hoyos L., Gonzalez J., Transient Internal Flow Characterization of a Bifurcated Submerged Entry Nozzle, *The Iron and Steel Institute of Japan International*, Vol. 46, 1183-1191, 2006.
- Teshima T., Kubota J., Susuki M., Ozawa K., Masaoka T., and Miyahara S., *Tetsu-to-Hagana*, Vol. 79 No. 5 576-582, 1993.
- Thomas B.G., Yuan Q., Sivaramakrishnan S. and Vanka S.P., Transient fluid flow in a continuous steel-slab casting mold, *The Minerals, Metals & Materials Society JOM-e*, 2002
- Thomas B. G. and Yu K. O., Modeling for casting and solidification processing, *Continuous Casting*, *Marcel Dekker*, 499-539, 2002.
- Thomas B.G. and Bai H., Tundish nozzle clogging – Application of computational models, 18rd Process Technology Division Conference Proceedings, Vol. 18, *Iron and Steel Society*, Warrendale, PA, 895-912, 2001a.
- Thomas B. G., Yuan Q., Sivaramakrishnan S., Shi T., Vanka S. P. and Assar M. B., Comparison of four methods to evaluate fluid velocities in a continuous slab casting mold, *The Iron and Steel Institute of Japan International*, Vol. 41, 1262-1271, 2001b.
- Yokoya S., Takagi S., Ootani S., Iguchi M., Marukawa K., Hara S., Swirling flow effect in submerged entry nozzle on bulk flow in high throughput slab continuous casting mold, *The Iron and Steel Institute of Japan International*, Vol. 4, No. 10, 1208-1214, 2001.
- Yokoya S., Takagi S., Iguchi M., Asako Y., Westoff R. and Hara S., Swirling effect in immersion nozzle on flow and heat transport in billet continuous casting mold, *The Iron and Steel Institute of Japan International*, Vol. 38, No. 8, 827-833, 1998.
- Zhang L., Yang S., Cai K., Li J., Wan X. and Thomas B.G., Investigation of fluid flow and steel cleanliness in the continuous casting strand, *Metallurgical and Materials Transactions B* Vol. 38b, 63, 2007.
- Zhang L., Aoki J., and Thomas B.G., Inclusion removal by bubble flotation in a continuous casting mold, *Metallurgical and Materials Transactions B*, Vol. 37b, 361-379, 2006.
- World Steel in Figures 2006, *International Iron and Steel Institute*, 2006.